Supporting Material

Transbilayer co-localization of lipid domains explained via measurement of strong coupling parameter

Matthew C. Blosser,[1] Aurelia R. Honerkamp-Smith,[2] Tao Han,[3] Mikko Haataja,[3] and Sarah L. Keller,[1]

[1]Departments of Chemistry and Physics, University of Washington, Seattle WA 98195-1700 USA
[2]Department of Applied Mathematics and Theoretical Physics, University of Cambridge, Cambridge CB3 0WA, UK
[3]Department of Mechanical and Aerospace Engineering, Princeton University, Princeton NJ 08544 USA

Contents:

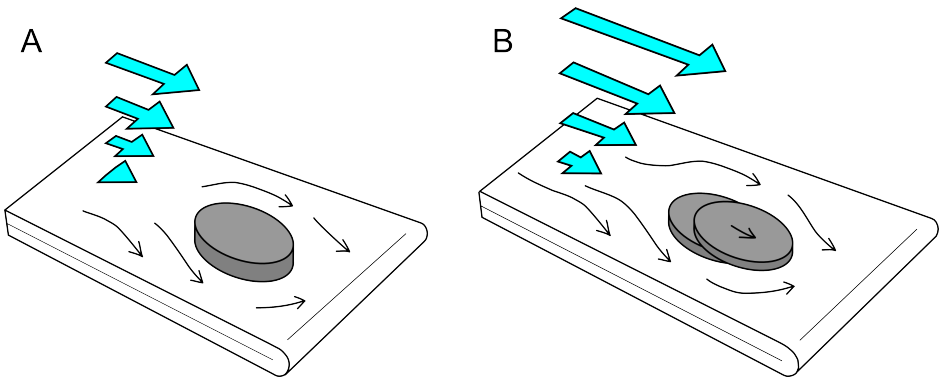

Figure S1: Schematic depicting the origin of forces favoring deregistration of an isolated domain. The shear force, F_{shear}, is caused by direct interaction with the solvent. The motion of the solvent is represented by the large blue arrows. The drag force, F_{drag}, is caused by the bulk membrane phase moving around the domain. The motion of the phase is represented by the small black arrows. (A) At low rates of flow, the shear in the solvent is low, and the velocity of the bulk phase is low. The domain remains stationary as the bulk phase moves around it. (B) At high rates of flow the shear in the solvent phase and the velocity of the bulk membrane phase both increase, driving the domain out of registry.

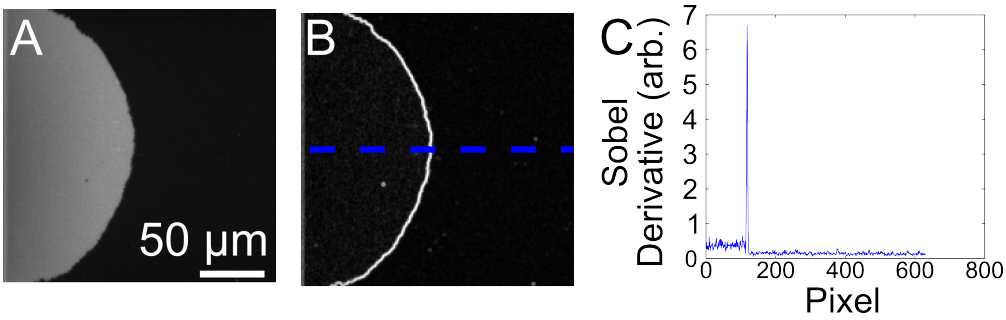

Figure S2: Automated edge tracking process. (A) Micrograph of the bilayer front. (B) A Sobel derivative of Panel A, where regions of high intensity correspond to the edge of the bilayer in Panel A. (C) A line scan along the blue dashed line (vertically averaged over the same thickness) in Panel B. The peak corresponding to the bilayer edge is clearly identifiable.

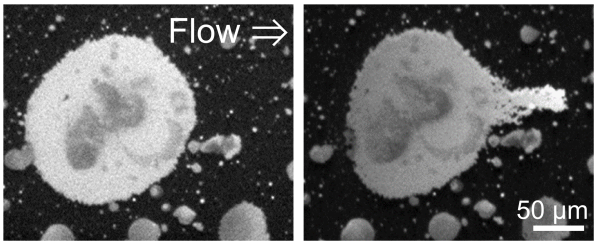

Figure S3: Ruptured GUV under flow. Black areas are bare glass. Dark gray areas within bright areas formed from ruptured GUVs are Lo domains. Under flow of buffer, only a narrow strip of bilayer is displaced at the front edge, while most of the bilayer edge remains pinned. This result illustrates why deregistration experiments in the main text used supported lipid bilayers produced from GUVs as well as SUVs, as shown schematically in Fig. 1 of the main text.

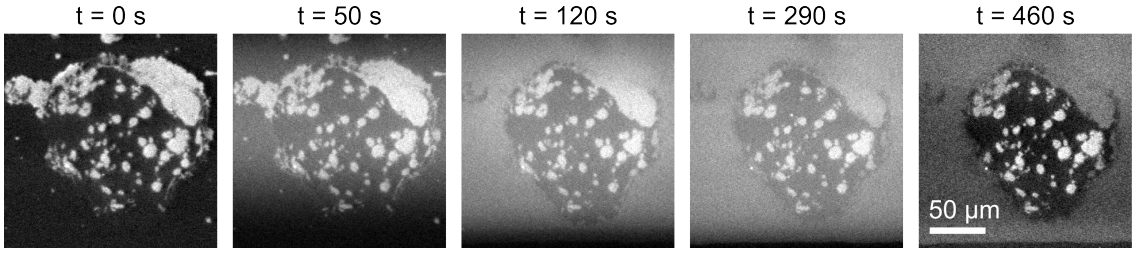

Figure S4: Lipids diffuse between adjoining supported bilayers formed from GUVs and SUVs. At t = 0 s a ruptured GUV of primarily dark, Lo phase is shown. At t = 50 s, SUVs with the same composition as the Ld phase, but half the concentration of fluorescent label, are shown flowing into the chamber as a diffuse bright band in the middle of the image. At t = 120 s, ruptured SUVs have formed a continuous supported bilayer, as evidenced by the diffusion of fluorophores that were initially in the Ld

domains at the perimeter of the ruptured GUV. At t = 290 s, the equilibration of these fluorophores concentrations is close to complete, and the Ld domains at the perimeter have nearly the same intensity as the surrounding Ld phase formed from ruptured SUVs. Ld domains in the interior appear brighter than the bulk phase because the low partitioning of the fluorophore to the intervening Lo phase slows equilibration. At t = 460 s, the majority of the unruptured, free-floating SUVs in solution have been rinsed out of the flow chamber. Because free-floating SUVs introduce high background fluorescence intensity, the brightness and contrast of each image was adjusted independently.

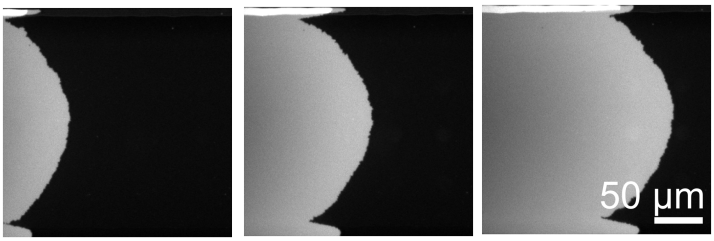

Figure S5: POPC bilayer under a bulk flow moving from left to right over a clean glass slide. The labeled bilayer was made from ruptured SUVs. The bulk flow rate from left to right is 0.22 mL/min, and each micrograph was taken at a 20-minute interval.

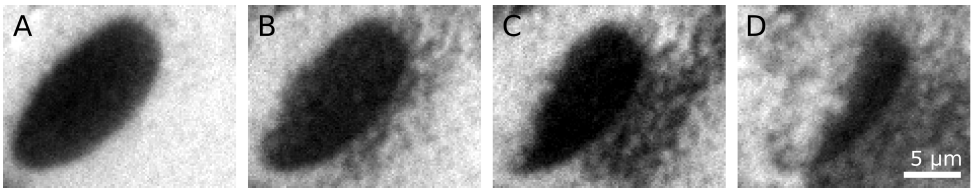

Figure S6: Evidence of domain deregistration for an oblong Lo domain before flow (left) and during application of 32 Pa of shear (right). In the cases shown in the main text, deregistered domains exhibit only two fluorescence levels because fluorophores partition to the top leaflet of the supported bilayer (1). The case in this figure is an exception. (A) The domain is initially in registry. (B) As the domain moves out of registry, three fluorescence levels are observed: a bright level corresponding to regions of Ld phase in both leaflets, a dark level corresponding to regions of Lo phase in both leaflets, and an intermediate level corresponding to a region of Lo phase in the top leaflet apposing a region of Ld phase in the bottom leaflet (the opposite case is more difficult to see). This initial onset of deregistration is used to determine the threshold shear. (C) As the domain moves further out of registry, the same changes drastically. (D) At long times, the presence of a domain in the lower leaflet is still apparent. As expected with a stationary lower leaflet, the boundary between the Lo phase and the Ld phase in the lower leaflet does not move significantly. Threshold shear values for domains exhibiting three fluorescence levels were in agreement with the fit in Fig. 6 of the main text.

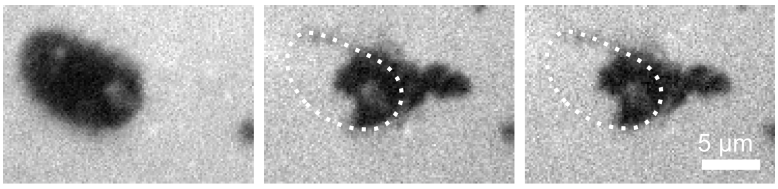

Figure S7: Partially registered domains do not spontaneously register in the absence of flow. The micrographs show a partially deregistered domain immediately after flow ceases and 10 min. after flow ceases. The dotted line shows the original position of the domain, which corresponds to the position of the Lo phase in the lower leaflet. No return to registration is observed.

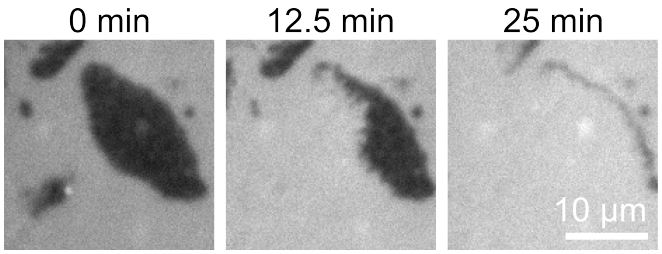

Figure S8: Illustration of why domains are not tracked over long times in this study. The micrographs show dark, putatively Lo domains under flow that increases from 0.44 mL/min to 0.88 mL/min over 25 minutes. The large domain at the right drastically changes in size, and the domain in the lower left is undetectable at late times.

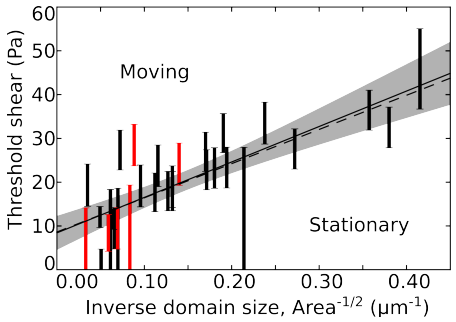

Figure S9: Threshold shear required to move Lo domains in the upper leaflet of a supported bilayer, as in Fig. 6 of the main text. Data from the six most irregularly shaped domains are highlighted in red. These domains were chosen because they contained smaller domains of the majority phase, their boundary was not smooth, and/or their overall shape was non-convex. To ensure that these points are consistent with the rest of

the data, we refit the line with the data in red removed (dashed line). The best-fit slope agrees within uncertainty to that obtained using the entire data set, changing Λ from 81 ± 22 Pa μm to 79 ± 23 Pa μm.

Calculating Shear

The behavior of flow in a channel is described by the Navier-Stokes equation. For a rectangular channel, the shear force τ on the bottom of the channel at a position z from the center line is given by

$$\tau(z) = -\frac{\Delta p}{\Delta x}\frac{h}{2}\left(1 - \frac{8}{\pi^2}\sum_{k\ odd}^{\infty}\frac{1}{k^2}\frac{\cosh(k\pi z/h)}{\cosh(k\pi w/2h)}\right)$$

$$\frac{\Delta p}{\Delta x} = -\frac{12\eta Q}{h^3 w}\left(1 - \frac{192}{\pi^5}\sum_{k\ odd}^{\infty}\frac{h\ \tanh(k\pi w/2h)}{w\ k^5}\right)^{-1}$$

where Q is the bulk flow rate, h is the height of the channel, w is the width of the channel, $\Delta p/\Delta x$ is the change in pressure in the direction of flow, and η is the viscosity of the aqueous phase (2, 3). This expression assumes no-slip boundary conditions, which is reasonable because the velocity of the supported bilayer is orders of magnitude smaller than the velocity of the bulk liquid in the channel (3). For domain deregistration experiments, we report the shear experienced by the domain center. For interleaflet friction measurements, we report the average shear as was reported in previous work (3). Our two channel geometries had widths of 224 μm and 214 μm. Both had a height of 105 μm. To calculate the shear, we truncated the series after the first 100 terms; including the next 100 terms would change the approximation by less than 1 part in 10^{-10}.

Derivation of λ_T for an isolated domain

The drag coefficient, λ_T, relates to the drag force via $F_{drag} = \lambda_T\, v_0$. Here, we derive the expression for λ_T, $\lambda_T \simeq \pi b_d R^2$, appropriate for the present problem for an isolated circular domain (solid or liquid) of radius R embedded within the upper leaflet. We focus on only the relevant regime in which the surrounding phase flows at a rate proportional to the applied shear. For a bilayer of pure DOPC, this regime corresponds to values of applied shear greater than ~3 Pa. Our data in Fig. 6 of the main text apply to this condition. To this end, our starting point is the Navier-Stokes equations for creeping flow of the incompressible fluid comprising the upper leaflet outside the domain ($r > R$),

$$\eta_M \nabla^2 \mathbf{v} - \nabla p + \tau \hat{\mathbf{x}} = b_d \mathbf{v}$$

and

$$\nabla \cdot \mathbf{v} = 0,$$

where $\mathbf{v}(\mathbf{r})$ denotes the velocity of the upper leaflet relative to the substrate, and η_M denotes the membrane viscosity (4-6). The presence of a shear stress τ in the solvent is accounted for by an effective body force $\tau\,\hat{\mathbf{x}}$ acting on the membrane. Far away from the domain, $\mathbf{v} \rightarrow v_0\,\hat{\mathbf{x}}$, where $v_0 = \tau / b_d$. Within the interior of the domain ($r < R$), the governing equations are given by

$$\eta'_M \nabla^2 \mathbf{v}' - \nabla p' + \tau \hat{\mathbf{x}} = b'_d \mathbf{v}'$$

and

$$\nabla \cdot \mathbf{v}' = 0.$$

At this point, the equations are valid for an arbitrary viscosity contrast between the domain and the Ld phase. Note that the special case of a solid domain is obtained upon taking the limit $\eta'_M \rightarrow \infty$ in the solution to the governing equations (6).

Now, the governing equations can be readily solved to yield

$$v_r = \left[v_0 - \frac{C_1}{r^2} - \frac{C_2}{r} K_1\left(\frac{\epsilon r}{R}\right) \right] \cos(\theta),$$
$$v_\theta = \left[-v_0 - \frac{C_1}{r^2} - \frac{C_2}{r} \left[\left(\frac{\epsilon r}{R}\right) K_0\left(\frac{\epsilon r}{R}\right) + K_1\left(\frac{\epsilon r}{R}\right) \right] \right] \sin(\theta),$$
$$p = -\frac{b_d C_1}{r} \cos(\theta)$$

and

$$v'_r = \left[v_0 - C'_1 + \frac{C'_2}{r} I_1\left(\frac{\epsilon' r}{R}\right) \right] \cos(\theta),$$
$$v'_\theta = \left[-v_0 + C'_1 - \frac{C'_2 \epsilon'}{R} I_0\left(\frac{\epsilon' r}{R}\right) + \frac{C'_2}{r} I_1\left(\frac{\epsilon' r}{R}\right) \right] \sin(\theta),$$
$$p' = -b'_d C'_1 r \cos(\theta)$$

in polar coordinates, with

$$\epsilon = R \sqrt{\frac{b_d}{\eta_M}}$$

and

$$\epsilon' = R \sqrt{\frac{b'_d}{\eta'_M}}.$$

Furthermore, $I_i(\epsilon')$ and $K_i(\epsilon)$ and denote the modified Bessel functions of the first and second kind, order i, respectively.

Following our earlier work (6), the 4 integration constants (C_1, C_2, C_1', C_2') are determined by imposing the continuity of shear stresses and velocity field along the domain boundary $(r = R)$, as well as requiring that the flow field within the domain vanishes on average; that is,

$$\int_0^R drr \int_0^{2\pi} d\theta \mathbf{v}'(r,\theta) = \mathbf{0}.$$

These requirements lead to the following expressions for the integration constants:

$$C_1 = v_0 R^2 \left[1 + 2\frac{K_1(\epsilon)}{\epsilon K_0(\epsilon)} + \frac{2K_1^2(\epsilon)\eta_M(I_0(\epsilon')\epsilon' - 2I_1(\epsilon'))}{K_0(\epsilon)M(\epsilon,\epsilon',\eta_M,\eta_M')}\right];$$
$$C_2 = 2v_0 R\left[-\frac{1}{\epsilon K_0(\epsilon)} + \frac{K_1(\epsilon)\eta_M(2I_1(\epsilon') - I_0(\epsilon')\epsilon')}{K_0(\epsilon)M(\epsilon,\epsilon',\eta_M,\eta_M')}\right];$$
$$C_1' = v_0\left[1 - \frac{2I_1(\epsilon')K_1(\epsilon)\epsilon\eta_M}{M(\epsilon,\epsilon',\eta_M,\eta_M')}\right];$$
$$C_2' = -\frac{2v_0 R\epsilon\eta_M K_1(\epsilon)}{M(\epsilon,\epsilon',\eta_M,\eta_M')}.$$

Here,

$$M(\epsilon,\epsilon',\eta_M,\eta_M') = (2K_0(\epsilon) + K_1(\epsilon)\epsilon)(2I_1(\epsilon') - I_0(\epsilon')\epsilon')\eta_M - K_0(\epsilon)\eta_M'(4I_1(\epsilon') - 2I_0(\epsilon')\epsilon' + I_1(\epsilon')\epsilon'^2).$$

[Note that the special case of a solid domain is obtained upon setting $\eta_M' \to \infty$ in the above expressions.] Finally, the drag force can be explicitly evaluated to yield

$$F_{drag} = 2R\int_0^\pi d\theta[(p - \tau_{rr})\cos(\theta) + \tau_{r\theta}\sin(\theta)]_{r=R}$$
$$= \pi v_0\left[\eta_M\epsilon^2 + \frac{4\epsilon K_1(\epsilon)\eta_M\left[(4+\epsilon'^2)I_1(\epsilon') - 2\epsilon' I_0(\epsilon') + 2\frac{\eta_M}{\eta_M'}(\epsilon' I_0(\epsilon') - 2I_1(\epsilon'))\right]}{K_0(\epsilon)[(4+\epsilon'^2)I_1(\epsilon') - 2\epsilon' I_0(\epsilon')] + \frac{\eta_M}{\eta_M'}(2K_0(\epsilon) + \epsilon K_1(\epsilon))(-2I_1(\epsilon') + \epsilon' I_0(\epsilon'))}\right]$$
$$\simeq \pi b_d R^2 v_0,$$

where the latter expression is valid for both solid and liquid domains in the limit $\epsilon, \epsilon' \gg 1$, corresponding to $R \gg 10^{-9}$m, relevant for our experiments. Thus, $\lambda_T =$

$F_{drag}/v_0 \simeq \pi b_d R^2$. Note that F_{drag} has the same magnitude as F_{shear}, but is a distinct force. Also note that λ_T, which is proportional to the coefficient of interleaflet friction b_d, is due to increased interleaflet interactions in the bulk membrane phase flowing around a stationary domain, and that the value of b_d does not depend on the material properties of the domain itself.

Effect of other domains on λ_T of a given domain

The effect of other domains on the drag coefficient of a particular domain can be estimated within an effective medium theory approach (7). To this end, we imagine that the other immobile domains act effectively as a porous medium in which the domain of interest is embedded, and the medium is endowed with effective permeability or friction coefficient $b_d + b_{eff}$. The governing equation is now written

$$\eta_M \nabla^2 \mathbf{v} - \nabla p_{eff} = \left(b_d + b_{eff}\right)\mathbf{v},$$

and the drag force on an isolated domain is computed. The magnitude of b_{eff} will be determined self-consistently at the end of the calculation. Following the steps in the analysis of an isolated domain readily yields $F_{drag} \simeq \pi R_i^2 v_0 (b_d + b_{eff})$.

Consider now N immobile domains within an $L \times L$ area of the upper leaflet. The net force acting on the domains is obtained by summing up the contributions from individual drag forces to yield

$$F_{tot} = \left(b_d + b_{eff}\right) v_0 \sum_{i=1}^{N} \pi R_i^2 = \left(b_d + b_{eff}\right) v_0 A_{tot}^{domain}.$$

On the other hand, for a porous medium whose behavior is governed by Darcy's law $-\nabla p = b_{eff}\mathbf{v}$, the pressure drop across the area is given by $\frac{\Delta p}{L} = b_{eff} v_0$. The total force exerted by the pressure drop on the particles is given by $\Delta p L = b_{eff} v_0 L^2 = F_{tot}$. Thus, $b_{eff} v_0 L^2 = \left(b_d + b_{eff}\right) v_0 A_{tot}^{domain}$, or

$$b_{eff} = b_d \frac{\phi}{1-\phi},$$

and

$$\lambda_T = \frac{\pi b_d R^2}{1-\phi},$$

where $\phi = A_{tot}^{domain}/L^2$ denotes the area fraction of the domains. It can be seen that the presence of the other domains increases the effective drag force on a particular domain.

Supporting References

1. Jönsson, P., J. P. Beech, J. O. Tegenfeldt, and F. Höök. 2009. Shear-driven motion of supported lipid bilayers in microfluidic channels. J. Am. Chem. Soc. 131:5294-5297.
2. Bruus, H. 2008. Theoretical Microfluidics. Oxford University Press, New York, NY.
3. Jönsson, P., J. P. Beech, J. O. Tegenfeldt, and F. Höök. 2009. Mechanical behavior of a supported lipid bilayer under external shear forces. Langmuir 25:6279-6286.
4. Evans, E., and E. Sackmann. 1988. Translational and rotational drag coefficients for a disk moving in a liquid membrane associated with a rigid substrate. J. Fluid Mech. 194:553-561.
5. Ramachandran, S., S. Komura, M. Imai, and K. Seki. 2010. Drag coefficient of a liquid domain in a two-dimensional membrane. Eur. Phys. J. E 31:303-310.
6. Han, T., T. P. Bailey, and M. Haataja. 2014. Hydrodynamic interaction between overlapping domains during recurrence of registration within planar lipid bilayer membranes. Phys. Rev. E 89:032717.
7. Brinkman, H. C. 1947. A calculation of the viscous force exerted by a flowing fluid on a dense swarm of particles. Appl. Sci. Res. A1:27.